

CHAPTER 20

THE EFFECT OF WAVE DIRECTIONALITY ON NEARSHORE WAVES

Michael J. Briggs and Jane M. Smith¹
Member and Associate Member, ASCE

ABSTRACT

A three-dimensional, physical model study of the effects of nonlinearity and wave directionality (i.e. directional distribution of energy or the directional spread of energy about a peak wave direction) on wave transformation in the nearshore region is presented. The model consisted of a 1:30 fixed bed beach with plane-parallel contours. Fifty-four irregular wave conditions, typical of unimodal and bimodal directional spectra, were simulated. Twenty capacitance wave gages formed offshore and nearshore linear arrays to measure directional distributions and a cross-shore array to study transformation of the frequency spectra. Both linear and nonlinear processes were observed in the transformed directional spectra. The primary effect of wave directionality was reduction in the strength of the nonlinear phase coupling between modes. Directional spreading also reduced the formation of subharmonics (i.e. long period energy) in the transformed spectra.

1.0 INTRODUCTION

The transformation of waves in shallow water is dependent on irregularity of the wave field. The wave field is composed of a variety of periods, heights, and directions, but little guidance exists on combined effects of energy and directional distributions on wave shoaling, refraction, and breaking.

Accurate nearshore wave predictions are critical for estimating beach evolution and designing coastal structures. Site-specific wave conditions in the nearshore

¹Research Hydraulic Engineer, USAE Waterways Experiment Station, Coastal Engineering Research Center, 3909 Halls Ferry Rd., Vicksburg, MS 39180.

region are difficult and expensive to acquire, so designers of coastal structures often rely on measurements taken offshore. These measurements are then transformed to the desired shallow-water location using linear, numerical models which include the effects of shoaling, refraction, and bottom friction (Jensen, et. al. 1987). Unfortunately, these numerical models do not include the effects of nonlinear wave-wave interactions and wave directionality.

Although incident nearshore wave energy is usually concentrated in a narrow band of frequencies and directions, measured spectra seaward of the shoaling region are often multi-modal in frequency with broad directional spreading (Long 1989). Waves in the shoaling region are both weakly nonlinear and dispersive.

Elgar and Guza (1985) found that nonlinear coupling between frequencies was a significant mechanism in the transformation of ocean surface gravity waves. Freilich, et. al. (1990) showed that linear theory inaccurately predicts both the shapes and total variances of directional spectra in shallow water. They also found that the "vector resonance conditions" for frequency and wavenumber accurately predicted directions of harmonics due to energy transfers from nonlinear, near-resonant triad interactions in the shoaling wave field. Elgar, et. al. (1990) showed that nonlinear effects observed in nonbreaking waves at Torrey Pines, California, could be successfully reproduced in a laboratory experiment.

Smith and Vincent (1990) conducted a series of flume tests on the shoaling and breaking of bimodal unidirectional wave spectra. They found that during wave decay, wave energy is lost preferentially in the higher frequency mode. The flume results also showed that relative "closeness" and distribution of energy between modes were important. These results support nonlinear wave-wave interactions as a mechanism for wave evolution.

Sand, et. al. (1983) measured diffracted wave energy in the lee of a model entrance breakwater and found larger waves for the directional cases. However, in model tests of wave transformation in the lee of a submerged mound, Vincent and Briggs (1989) found the unidirectional waves higher than equivalent directional waves. Bowers (1987) found that directional spreading significantly reduced the long period energy associated with wave grouping in harbor modelling. Hasselman, et. al. (1963) found that directional spreading and uncoupled waves at harmonic frequencies decreased the measured nonlinearity.

Thus, inclusion of nonlinear transformation processes and wave directionality can have a significant effect on

coastal design by providing more realistic estimates of nearshore conditions. The results of these tests will be used to upgrade numerical wave transformation models for predicting nearshore wave properties from offshore measurements or hindcasts.

In this paper, the experimental setup is described in section 2. In section 3, the wave and test conditions for the 54 unimodal and bimodal, frequency and directional distributions are presented. Data collection and analysis procedures are described in section 4. Section 5 describes preliminary tests conducted to calibrate the model and control signals. Transformation of the directional spectra is discussed in section 6. Finally, conclusions are contained in section 7.

2.0 EXPERIMENTAL SETUP

A three-dimensional, physical model of a gently sloping beach with plane, parallel contours (Fig. 1) was constructed in CERC's 28 m by 40 m directional spectral wave basin. The model scale for the 1:30 slope fixed bed model was approximately 1:25. The toe of the slope was located 4.5 m in front of the directional spectral wave generator (DSWG), in a water depth of 50 cm. The rear of the basin was lined with wave absorber backed by a concrete wall. The basin sides were lined with absorber and open to adjacent basins. Thus, wave energy was able to propagate away from the test area into adjacent larger basins with minimal reflections from distant vertical walls and associated basin cross-seiching.

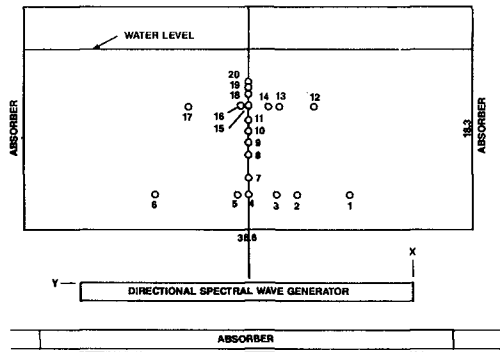


Fig. 1. Experimental Set-Up

Twenty capacitance wave gages were arranged in patterns and water depths similar to the prototype arrays used in 1978 and 1980 field experiments at Torrey Pines Beach, California (Pawka 1982). The gage pattern consisted of two 8-1-3-2-5 longshore linear arrays to measure changes in directional distributions and a cross-shore array to study frequency spectral evolution. The offshore (OGA) and near-shore (NGA) linear arrays were located in water depths of 40 cm and 16 cm, respectively. Lag spacings between gages for the OGA and NGA were 85 cm and 55 cm, respectively. The design of these arrays allowed measurements of waves with a directional resolution of approximately 8 deg (Pawka 1983). The cross-shore gage array (CSA) was nested within these two linear arrays, transverse to their axes and aligned with the physical model centerline. The spacing between the ten CGA gages was not uniform, varying between 0.5 to 2.0 m.

3.0 WAVE CONDITIONS

A total of 54 directional spectra were simulated as the product of the TMA shallow-water spectral form and a wrapped normal spreading function (Briggs, et. al. 1987). Both unimodal and bimodal frequency spectra with varying energy distributions were tested. The ratios of energy between modes in the bimodal spectra were 1/3:2/3, 1/2:1/2, and 2/3:1/3. Directional distributions were both narrow and broad and varied between modes. Target directional spectral parameters for individual modes were: $T_p = 1.25, 1.75, \text{ and } 2.50 \text{ sec}$ ($f_p = 0.40, 0.57, \text{ and } 0.80 \text{ Hz}$, respectively); $H_{m0} = 6.5, 7.6, 10.8, 12.2, 13.2, \text{ and } 15.2 \text{ cm}$; $\gamma = 3.3 \text{ or } 20.0$; $\theta = 0$ (shore-normal) and 20° ; and $\sigma_m = 0$ (unidirectional), 20 , and 40° . Wave direction is the angle towards which the waves travel, with positive angles measured clockwise from the normal to the DSWG.

These 54 wave conditions were converted into stroke control signals for each of the 61 paddles of the DSWG using a frequency domain, double summation, deterministic amplitude, random phase model. Typically, control signals were digitized at 20 Hz for 750 sec. After Fourier transformation in the frequency domain, this signal duration corresponded to an evenly-spaced frequency increment $\Delta f = 0.00133 \text{ Hz}$, or 1464 frequencies between the lower and upper cutoff frequencies $f_l = 0.05$ and $f_u = 2.00 \text{ Hz}$, respectively.

4.0 DATA COLLECTION & ANALYSIS

The wave gages were calibrated daily with a computer-controlled procedure incorporating a least square fit of measurements at 11-steps. After a waiting time of 20 sec to allow slower traveling high-frequency components to

reach the shallowest gages, surface elevation data were sampled at 10 Hz (i.e. $\Delta t = 0.10$ sec).

Data analyses consisted of single channel frequency spectral analysis for the CGA gages and directional spectral analysis for the OGA and NGA linear arrays. Data records of 500 sec were zero-meanded, tapered by a 10% cosine bell window, Fourier transformed, and band averaged, yielding a frequency resolution $B_e = 0.024$ Hz and $V = 24$ degrees of freedom. For the directional spectral analysis, the measured data again were zero-meanded, windowed, and Fourier transformed to the frequency domain. A Gaussian smoothing function then was used to smooth the cross-spectral matrix of auto- and cross-spectra with approximately $V = 56$. A high-resolution Maximum Likelihood Method (MLM) estimator was used to solve for the Fourier coefficients of the directional spreading function.

5.0 PRELIMINARY TESTS

Prior to wave transformation tests, three preliminary test phases were conducted: basin circulation, signal duration, and signal calibration. Based on current meter measurements and dye and visual observations, wave-induced circulation was not judged significant. In the second phase, measured spectral characteristics from test durations of 200 waves and 400 waves at the peak period were compared to determine proper sampling duration. Wave period, height, and spectral shape variations were within 95% confidence limits, so the shorter duration of 200 waves was selected for further tests. In the signal calibration phase, a frequency domain transfer function (Briggs and Jensen 1988) was used to iteratively correct the measured OGA spectra for variations in target peak period, wave height, and spectral shape.

The agreement between measured and target frequency spectra was very good to excellent. The peak of the measured spectra was often slightly smaller than the target spectra, but within 95% confidence limits. The maximum variation in peak frequency was ± 0.04 Hz (i.e. 2 frequency bands), occurring in only two cases. In most cases there was no significant difference between target values. Wave heights matched target values within 8% for all 54 cases. The agreement between measured and target directional distributions was good to excellent. The agreement for the unidirectional cases was excellent. The directionally spread cases, however, exhibited much more variability, with the measured results somewhat narrower than target distributions. Probable explanations are the resolving power of the arrays and MLM analysis technique and refractive-narrowing between the DSWG and OGA.

6.0 WAVE TRANSFORMATION RESULTS

Since it is impractical to present the results from all 54 cases (Briggs, et. al. 1990), three representative cases will be discussed in detail. The first case is a unimodal, unidirectional spectrum, representative of narrow-banded swell. The second case is a bimodal case, composed of two crossing, narrow-banded (in both frequency and direction) wave trains. The third example is another bimodal case, narrow-banded in frequency and broad-banded in direction. This last case is typical of a sea and swell spectrum with greater energy in the swell peak.

In the paragraphs below, the OGA and NGA directional spectra are presented to illustrate the spectral evolution between linear gage arrays. Next, the frequency spectra from the CGA provide greater detail on the energy transfers closer to shore. Since linear theory does not predict the formation of harmonics, bicoherence spectra from bispectral analysis are used to confirm the presence of nonlinear wave-wave interactions in the shoaling waves. Finally, peak wave period and significant wave height are discussed.

6.1 OGA Directional Spectra

MLM estimates of the directional spectra at the OGA for each of these three cases are shown in Fig. 2. The right vertical panel shows the frequency spectrum obtained by summing energy at each frequency over all directions. The left rear panel is the direction spectrum obtained in a similar manner, except that direction is held fixed and energy is summed over all frequencies. Frequency lines have variable spacing and are denser around the peaks and direction lines are spaced every 2° .

The first case (Fig. 2a) shows a single narrow peak, approaching the beach normally and centered at ($f_p = 0.40$ Hz, $\theta = 0^\circ$). Measured H_{m0} was 7.4 cm. The second example (Fig. 2b) shows a bimodal spectrum with crossing modes centered at ($f_{p,1} = 0.40$ Hz, $\theta_1 = 0^\circ$) and ($f_{p,2} = 0.57$ Hz, $\theta_2 = 20^\circ$), respectively. Measured H_{m0} was 8.4 cm, with a target distribution of 6.5 cm in each mode. A small secondary peak is observed centered at (0.57 Hz, 0°) which may be an artifact of the MLM estimation procedure or due to nonlinear effects on the spectra between the DSWG and the OGA. The third case (Fig. 2c) shows two shore-normal peaks centered at ($f_{p,1} = 0.40$ Hz, $\theta_1 = 0^\circ$) and ($f_{p,2} = 0.57$ Hz, $\theta_2 = 0^\circ$), with different amounts of full-width directional spreading ($\sigma_{m,1} = 20^\circ$, $\sigma_{m,2} = 40^\circ$). Measured H_{m0} was 13.1 cm. Wave refraction produced narrowing of the wider directional distributions by 6 to 10 deg between the DSWG and the OGA. Target wave heights were small enough to prevent wave breaking between the DSWG and the OGA.

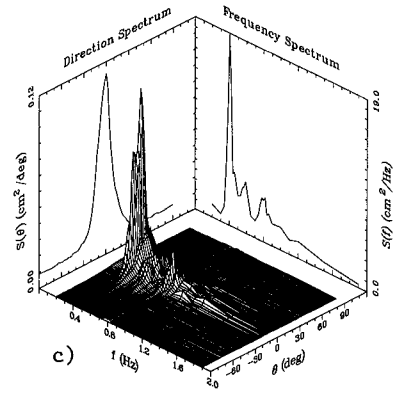
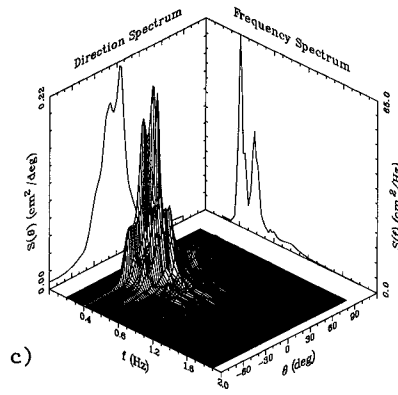
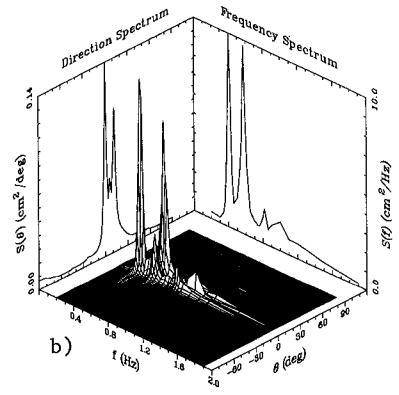
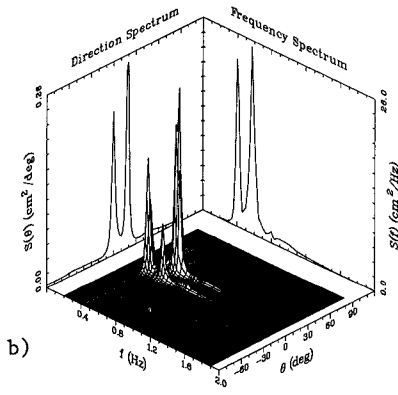
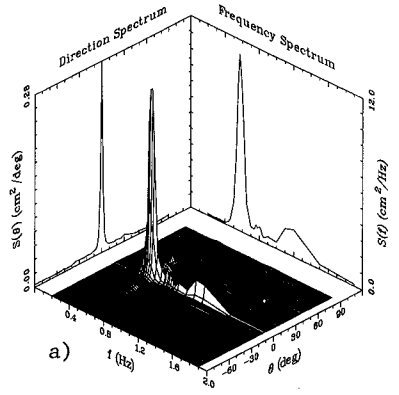
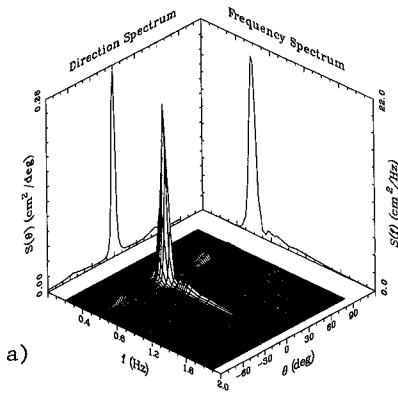


Fig 2. OGA Directional Spectra

Fig 3. NGA Directional Spectra

6.2 NGA Directional Spectra

Fig. 3 shows the NGA directional spectra for the three example cases. Fig. 3a for the first case indicates two distinct concentrations of energy: the narrow, unidirectional peak centered at (~ 0.57 Hz, 0°) and a broad, high frequency peak at (~ 1.14 Hz, 0°). Measured H_{m0} was 7.77 cm, indicating that the wave had not yet begun to decay. The transformed directional spectrum for the second case (Fig. 3b) shows five concentrations of energy: the low frequency peak centered at (~ 0.40 Hz, 0°); the high frequency peak at (~ 0.57 Hz, 10°); the "artifact" peak at (~ 0.57 Hz, 0°); a narrow harmonic peak at (~ 0.80 Hz, 0°); and a wider peak at (~ 0.97 Hz, 5°). The spectral energy is more shore-normal and the low-frequency, first mode appears to have gained energy at the expense of the high-frequency, second mode. This wave was still in the shoaling region because its measured H_{m0} was 8.74 cm. Finally, three concentrations of energy are evident (Fig. 3c) for the third case: the first mode centered at (~ 0.40 Hz, 0°); the remnant of the second mode at (~ 0.57 Hz, 0°); and a harmonic at (~ 0.80 Hz, 0°). The low-frequency peak has maintained its energy at the expense of the high-frequency peak, similar to observations in Smith and Vincent (1990). The measured H_{m0} for this last case was 11.68 cm, indicating that it was in the decay region of the surf zone.

The wave fields have transformed significantly between the two gage arrays. In general, the peaks are narrower and closer to shore-normal than the OGA spectra. Linear wave refraction accounts for approximately $10\text{--}14^\circ$ of the observed narrowing of the directional distributions. Wave breaking was observed between the OGA and NGA for all cases. The extent and initial location varied as a function of the target wave energy, being closer to shore for the initially smaller wave heights.

6.3 CSA Frequency Spectra

The NGA directional spectra suggested the formation of harmonics as the waves shoaled between deep and shallow arrays. Greater detail of this spectral evolution can be found by studying the frequency spectra from the CGA gages. Fig. 4 shows semi-log plots of the measured frequency spectra for two gages in the CGA: gage 4 (center of the OGA and incident conditions) and gage 20 (closest to shore). Corresponding water depths were 40.0 and 9.5 cm, respectively.

The first case (Fig. 4a) shows energy transfers from the peak frequency at (0.57 Hz) to second (~ 0.114 Hz) and third (~ 1.71 Hz) harmonics as the wave shoals. The fourth subharmonic (~ 0.14 Hz) experiences a fivefold increase in energy. The second case (Fig. 4b) supports the growth of

harmonics seen in the NGA directional spectrum (Fig. 3b), and suggests even higher harmonic growth at (~ 1.14 Hz, ~ 1.37 Hz, and ~ 1.71 Hz). Subharmonics at the difference frequency between modes (~ 0.17 Hz) and the second mode (~ 0.28 Hz) are indicated. The third case (Fig. 4c) becomes unimodal as it transforms; the "spectral valley" originally between first and second modes disappears. At a depth of 29.3 cm (not shown), energy is initially transferred to the harmonic frequency corresponding to the summation of mode frequencies (~ 0.97 Hz). By the time the wave travels to 9.5 cm depth, energy is transferred out of this harmonic and the second mode ($f_{p,2} = 0.57$ Hz) to the second and third harmonics of the first mode peak at (~ 0.80 Hz and ~ 1.20 Hz). The two subharmonic peaks present in the second case have coalesced into a single peak at the difference frequency at (~ 0.17 Hz).

6.4 Bispectral Analysis

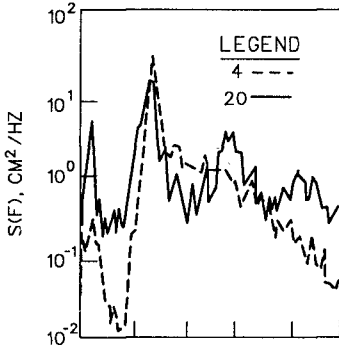
From the previous two sections, it is obvious that both linear and nonlinear processes are responsible for the observed changes in transformed wave spectra. Linear theory does not predict the growth of harmonics during wave shoaling. One method used to detect these nonlinear wave-wave interactions is bispectral analysis. The bispectrum (third-order spectrum) is a useful tool because only phase-coupled components appear. In the absence of this quadratic phase coupling (i.e. mode independence), the bispectrum is zero. Two wave components are harmonically related (i.e. dependent) if their interaction transfers energy at their sum and/or difference frequencies. A special case is harmonics at an integer multiple of a primary mode. The "vector resonance conditions" define this nonlinear, near-resonant triad interaction phenomenon. Both the frequencies f_i and vector wavenumbers k_i must sum to nearly zero and are given by

$$f_3 = f_1 \pm f_2 \quad (1a)$$

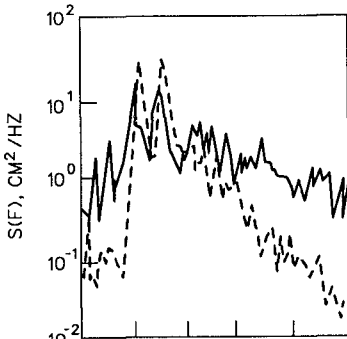
$$k_3 = k_1 \pm k_2 \quad (1b)$$

Freilich, et. al. (1990) showed that these conditions accurately predicted phase coupling between wave trains at Torrey Pines, California, approaching the beach at different directions, with energy transferred to a third mode corresponding to the sum frequency and vector sum direction.

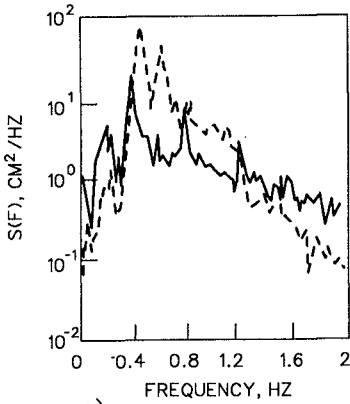
Fig. 5 shows the measured bicoherence spectra for our three example cases at gage 20 (9.4 cm). Because of the short durations of collected data, the number of degrees of free-



a)

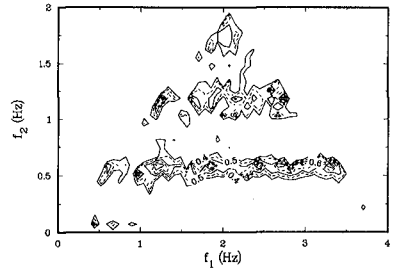


b)

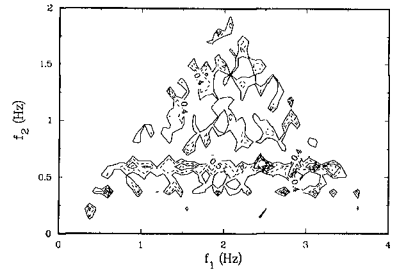


c)

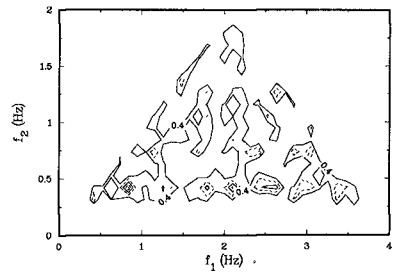
Fig 4. CGA Frequency Spectra



a)



b)



c)

Fig 5. Bicoherence Spectra

dom for the bispectral analysis is only 58 or 82. Elgar and Guza (1985) recommended $N = 150$ to 300 to improve statistical stability for field data. The minimum contour in the figures is at 0.4, with additional contours at 0.1. The first case (Fig. 5a) has bicoherence maxima (strong nonlinear interactions) between the first mode and its harmonics at $(f_2 = 0.57, f_1 = 0.57)$, $(0.57, 1.14)$, $(0.57, 1.71)$, $(0.57, 2.28)$, $(0.57, 2.85)$, and $(0.57, 3.42)$. Also, the second (1.14 Hz) and third (1.71 Hz) harmonics show similar strong nonlinear phase coupling among themselves and their harmonics. The third frequency f_3 of each triad is the sum of the two in parentheses. The bicoherence peak at $(0.57, 0.57)$ is the self-self-second harmonic triad observed in Figs. 3a and 4a at (1.14 Hz, 0°). It satisfies the "vector resonance condition" since $f_2 = f_1$, $f_3 = 2f_1 = 2(0.57) = 1.14$ Hz, and the wavenumber of the second harmonic is oriented in the same direction (0°) as the first mode.

Fig. 5b shows the bicoherence spectrum for the second example case. The phase coupling is more confused than the previous case due to the addition of the second mode and the non-aligned directions of the wave trains, although the horizontal trends at the two primary modes is similar to Fig. 5a. Bicoherence maxima are observed at $(0.17, 0.28)$, $(0.40, 0.57)$, $(0.40, 0.97)$, $(0.57, 0.57)$, $(0.57, 0.80)$, and $(0.57, 1.14)$. The first set corresponds to an apparent nonlinear interaction of the subharmonics of the difference frequency between primary modes and the second subharmonic of the second mode (Fig. 4b). This is indicative of the low-frequency phenomenon "surf beat" composed of infragravity modes. The second triad corresponds to the peak at $(0.97, 5^\circ)$ in Fig. 4b, at the sum frequency of the primary modes and the direction corresponding to the approximate vector sum of the wavenumbers. Peaks corresponding to the third frequency of the remaining triads can be seen in the high frequency portion of Fig. 4b. Lack of sufficient degrees of freedom in the bispectral analysis and non-alignment of wave directions in the primary modes might explain why the peak at $(0.80$ Hz, $0^\circ)$ does not show a strong nonlinear coupling in the bicoherence spectrum.

The bicoherence spectrum for the third case is shown in Fig. 5c. In this case, energy is narrow-banded in frequency but broad-banded in direction with aligned wave directions normal to the beach. Elgar and Guza (1985) found that directional spreading produced a weaker bicoherence spectrum. Bicoherence maxima are located at $(0.40, 0.40)$, $(0.40, 0.57)$, $(0.40, 0.80)$, and several higher harmonics. The first triad represents the self-self-second harmonic degenerate triad which produces the second harmonic at $(0.80$ Hz, $0^\circ)$ observed in Figs. 4c and 5c. The second triad is the harmonic at $(0.97$ Hz, $0^\circ)$ due to the sum of

the first and second modes. The nonlinear interaction of the primary (0.40 Hz, 0°) with the nonlinearly-generated second harmonic at (0.80 Hz, 0°) produces the third harmonic at (1.20 Hz, 0°). The "vector resonance conditions" are again satisfied since all components are collinear at 0° . Also, the growth of subharmonics seems to be suppressed relative to the first two cases without directional spreading.

6.5 Wave Period and Height Transformation

Peak wave periods in the CGA showed little change. Typically, they remained invariant or shifted slightly to a lower frequency. Since the resolution bandwidth is 0.024 Hz, some of this frequency variation is explained by statistical variability.

As the waves shoaled, wave height initially remained fairly flat or increased slightly. Inside the surf zone (decay region), wave height became locally depth controlled, no longer governed by outside (deep water) conditions, as the waves became saturated. Fig. 6 shows these trends for the CGA gages for 38 cases with target wave heights of 15.2 cm. The first two example cases have been omitted since the shoaling region extended throughout most of the model slope (i.e. closer to shore). A fourth degree polynomial, least square fit to the data is also shown for illustrative purposes. The fitted curve has been smoothed using locally weighted scatterplot smoothing (Cleveland 1979, 1981) which uses a weighted average of the nearby y values.

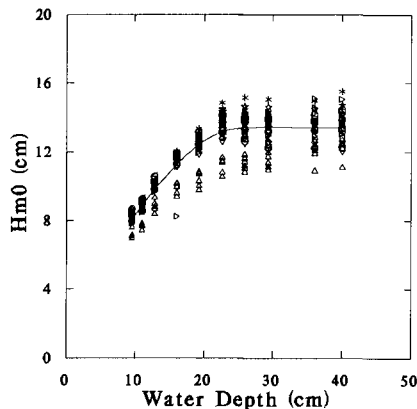


Fig 6. Wave Height vs. Depth

7.0 CONCLUSIONS

These tests have demonstrated that realistic ocean wave fields can be reproduced in a controlled laboratory experiment to study the mechanisms which effect transformation of nearshore waves. Both linear and nonlinear processes were observed in the shoaled directional spectra. The primary effect of wave directionality was reduction in the strength of the nonlinear phase coupling between modes, more so for directional spreading than wave direction. Directional spreading also reduced the formation of subharmonics (i.e. long period energy) in the transformed spectra.

ACKNOWLEDGEMENTS

The authors wish to acknowledge the Office, Chief of Engineers, U.S. Army Corps of Engineers, for authorizing publication of this paper. It was prepared under the Coastal Flooding and Storm Protection Program of the Civil Works Research and Development Program, managed by Dr. C. Linwood Vincent. We would like to thank Ms. Debra Green, Mr. David Daily, and Mr. Larry Barnes for their assistance. Dr. Charles Long made many helpful suggestions which were greatly appreciated. Dr. Steve Elgar, Washington State University, developed the bispectral analysis software.

REFERENCES

- Bowers, E.C. 1987. "Short Crested Seas in Harbor Modeling," Report No. SR 141, Hydraulics Research Limited, Wallingford, England, pp 24.
- Briggs, M.J., Borgman, L.E. and Outlaw, D.G. 1987. "Generation and Analysis of Directional Spectral Waves in a Laboratory Basin," Paper OTC 5416, Offshore Technology Conference, Houston, TX.
- Briggs, M.J. and Jensen, R. 1988. "Simulation of Extreme Storm Events in Coastal Structural Models," OSDS '88, Oregon State University, Corvallis, September, pp 119-133.
- Briggs, M.J., Smith, J.M., and Green, D.R. 1990. "Wave Transformation over a Generalized Beach," CERC Technical Report (in Press), USAE Waterways Experiment Station, Vicksburg, MS.
- Cleveland, W.S. 1979. "Robust Locally Weight Regression and Smoothing Scatterplots," J. ASA, 74, 829-836.
- Cleveland, W.S. 1981. "LOWESS: A Program for Smoothing Scatterplots by Robust Locally Weighted Regression," Am. Stat. 35, 54.

Elgar, S. and Guza, R.T. 1985. "Observations of Bispectra of Shoaling Surface Gravity Waves," JFM, Great Britain, 161, 425-448.

Elgar, S., Guza, R.T., Freilich, M.H., and Briggs, M.J. 1990 (Submitted). "Laboratory Simulations of Directionally Spread Shoaling Waves," J. WPCOE.

Freilich, M.H., Guza, R.T., and Elgar, S.E. 1990. "Observations of Nonlinear Effects in Directional Spectra of Shoaling Gravity Waves," JGR, 95(C6), June, 9645-9656.

Hasselmann, K., Munk, W., and MacDonald, G. 1963. "Bispectra of Ocean Waves," In Time Series Analysis (Ed. M. Rosenblatt), Wiley, pp 125-139.

Jensen, R.E., Vincent, C.L., and Abel, C.A. 1987. "A User's Guide to SHALWV: Numerical Model for Simulation of Shallow Water Wave Growth, Propagation, and Decay," Report 2, USAE Waterways Experiment Station, Vicksburg, MS.

Long, C.E. 1989. "Directional Characteristics of Waves in Shallow Water," Technical Report (In Publication), USAE Waterways Experiment Station, Vicksburg, MS.

Pawka, S.S. 1982. "Wave Directional Characteristics on a Partially Sheltered Coast," Ph.D. dissertation, UCSD, La Jolla, CA.

Pawka, S.S. 1983. "Island Shadows in Wave Directional Spectra," JGR, 88, 2579-2591.

Sand, S.E., Kirkegaard, J., Larsen, J., and Rodenhuis, G.S. 1983. "Numerical and Physical Modeling of Directional Diffraction of Waves," Coastal and Port Engineering in Developing Countries, Colombo, March.

Smith, J.M. and Vincent, C.L. 1990 (Submitted). "Shoaling and Decay of Two Wavetrains on a Beach," J. WPCOE.

Vincent, C.L. and Briggs, M.J. 1989. "Refraction-Diffraction of Irregular Waves Over a Mound," J. WPCOE, 115(2), March, 269-284.